Journal of Materials Chemistry B

Accepted Manuscript

ROYAL SOCIETY OF CHEMISTRY

www.rsc.org/materialsB

Journal Name

RSCPublishing

ARTICLE

Using Oxidant Susceptibility of Thiol Stabilized Nanoparticles to develop an Inflammation Triggered Drug Release System

Cite this: DOI: 10.1039/x0xx00000x

Received 00th January 2012,
Accepted 00th January 2012

DOI: 10.1039/x0xx00000x

www.rsc.org/

Faheem Muhammad,[a,b] Wenxiu Qi,[b] Aifei Wang,[a] Jingkai Gu,[b] Jianshi Du*[,c] Guangshan Zhu*[,a]

Inflammation is a complex and dynamic defensive cellular approach to safeguard against deleterious agents, however, overexpression of such responses frequently results in the development of number of devastating diseases, such as atherosclerosis, cancer, inflammatory bowel, Alzheimer's and Parkinson's diseases. At the site of inflammation, excessive amount of reactive oxygen species (ROS) are produced and therefore researchers are now earnestly trying to exploit ROS pathological signals to design oxidative triggered drug release systems. In this study, we report a straightforward strategy to develop an oxidative stress responsive drug release systems. Newly developed, ultrasmall, and thiol stabilized zinc sulfide quantum dots (ZnS QDs) are used as a nanocaps to regulate the release of anticancer drug (camptothecin) from mesoporous silica nanoparticles (MSNs) in response to oxidative environment. Exposure of capped nanocarrier to higher concentration of H_2O_2 fails to open the drug loaded nanochannels, however, an addition of a minute amount divalent iron, the most abundant transition-metal in the body, readily unseals the nanochannels at quite lower H_2O_2 concentrations due to the generation of highly reactive hydroxyl radicles (•OH). Thiol groups which stabilizes the ZnS nanolids are actually oxidized by •OH and as a result unleashes the loaded drug molecules from the channels of silica. Besides inflammation-induced drug delivery, this study also provides basic insight into the fate of thiol stabilized nanoparticles upon interaction with hydroxyl radicles.

1. Introduction

Reactive oxygen species (ROS) are ubiquitously produced in all living beings as byproducts of aerobic metabolism, and are recognized to play diverse kinds of biological and biochemical roles.[1-4] They are typically known for their deleterious roles and are associated with numerous diseases including inflammatory pathologies, tumors, cardiovascular and degenerative diseases.[5-10] Under normal cellular environment, there is a strict regulation between the generations and detoxification of ROS, as cells have number of antioxidant enzymes and non-enzymatic molecules namely superoxide dismutase (which reduces $O^{2-}$to H_2O_2), glutathione peroxidase, catalase, protein thiols, GSH, vitamin C, and vitamin E to detoxify reactive metabolites.[11] However, if disproportionate production of ROS overpowers the antioxidant defense system, cells are termed to be in a state of oxidative stress.[12-16] Among various ROS, superoxide radicle (O^{2-}) is a primary intracellular ROS that has the ability to trigger a cascade of reactions to produce "secondary" species, either through enzyme or metal-catalyzed reactions.[17] For instance, dismutation of superoxide yields a less reactive H_2O_2, but the stability and fat solubility of H_2O_2 endow it a further freedom to diffuse from the site of origin to distant part for executing different roles.[18-21] It is worth mentioning that the most of the H_2O_2 induced biomolecular damage is actually elicited by its transformation to more lethal and reactive species. H_2O_2 is readily transformed into hypochlorous acid (HOCl) in the presence of myeloperoxidase enzyme.[9] Under stress conditions, superoxide discharges Fe^{2+} ions from iron-chelating biomolecules to mediate the generation of highly reactive species, hydroxyl radicals (•OH),

via Fenton reaction.[22-25] Due to the presence of exceptionally reactive single unpaired electron, •OH have the capacity to react with all biomolecules and consequently causes severe cellular damages including lipid peroxidation, protein denaturing and membrane destruction. Another key reason behind its indiscriminate destructive nature is the lack of any intracellular enzymatic mechanism to tackle reactive radicles; therefore, excessive production of •OH invariably leads to cell death.

Besides H_2O_2 and O^{2-} involvement in the generation of reactive •OH, the availability of redox active metals, particularly iron, is also indispensable for catalyzing this reaction; otherwise the rate of uncatalyzed reaction is negligibly low. Iron is a bio-essential element which is found in safe chelated forms to participate in various biological functions, especially in oxygen transport. Intracellular concentration of iron is largely regulated within desirable limits to maintain redox potential of the cell, however, as mentioned above, superoxide induced free iron is highly prone to participate in Fenton reaction. Considerable and wide-ranging evidence linked the enhanced levels of poorly liganded iron in the body with large number of inflammatory disorders.[26-32] Inflammation is basically a tissues attempt at self-protection against virulent stimuli but its malfunctioning ubiquitously results in an initiation and progression of various diseases, such as arthritis, cancer, diabetes, heart disease, irritable bowel syndrome, Alzheimer's disease, Parkinson's disease, and many others.[33-35] It has been assessed that one human cell is under the attack of about 1.5×10^5 oxidative strikes per day from •OH and other reactive species.[36] Furthermore, there is a well-established relation between inflammations and cancer, microenvironment of cancer mostly contains inflammatory cells. Inflammatory cells produce prodigious amount of ROS and the presence of immune cells in tumor microenvironment also underlines the need for fabrication of •OH mediated drug delivery system to specifically target cancer microenvironment. To effectively treat •OH induced inflammatory diseases and cancer; oxidant responsive drug carriers are highly desirable to achieve specific release of therapeutic molecules.

Thanks to recent advances in nanotechnology, countless nanoparticle based stimuli responsive architectures have been developed.[37-40] Previously, polymers-based responsive nanoparticles were at the forefront to attain environmental specific drug release but due to susceptible nature of polymers to harsh biological conditions, researchers have shifted their focus towards the development of more robust and stable nanocarriers. Porous silica is emerged as an ideal alternative due to multitude of reasons.[41-42] Mesoporous silica nanoparticles (MSNs) are largely noted for their large surface area and tunable pore structure, moreover, they also possesses some unique features, such as excellent biocompatibility, high surface area, ready cellular uptake and controlled release behavior, which warrants its use in a wide range of biomedical applications. Above all, the presence of internal porous structure for loading of therapeutic cargo and external surface offers an unprecedented opportunity to manipulate the release of therapeutic entities according to environmental signals. Due to such versatility, several mesoporous silica based responsive drug delivery systems have been reported using various gatekeepers to regulate the release of drug molecules in response both endogenous and exogenous stimulations. Predominant triggers which have so far been explored are temperature, pH,[43] redox,[44] electric field,[45] light,[46] magnetic field[47] and competitive binding etc.

Oxidant responsive drug delivery is indeed of great therapeutic importance but until now very little research activity has been witnessed in this direction and even those studies are limited to polymer domain. Moreover, the focal point of previous reports were H_2O_2 responsive system and accordingly different H_2O_2 sensitive polymers such as boronate esters linkers,[48] poly (propylene sulfide),[49] polythioether[50] and selenium containing polymers[51]were used to regulate drug release. In this investigation, we develop an inflammation responsive mesoporous silica based drug delivery system using thiol stabilized ZnS nanoparticles as nanolids to block the release of loaded cargo. As most of the cancer cells demonstrate augmented ROS generation capacity due to unusual metabolic needs for uncontrolled proliferation and oncogenic stimulation, thus ROS signals can judiciously be used for the treatment of cancer[16, 52, 53] Anticancer drug camptothecin (CPT) is loaded into the nanochannels of MSNs prior to capping of nanochannels with ZnS QDs. The opening protocol and delivery of CPT molecules is based upon the oxidation of thiol groups, which passivate the ZnS nanolids, when highly reactive hydroxyl radicals via metal-mediated reactions are introduced into nanosystem. The synthetic and working protocol of inflammation responsive drug delivery system is illustrated in Scheme 1.

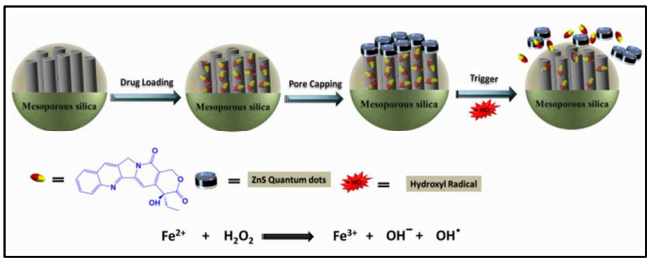

Scheme 1. Schematic representation of synthetic and working mechanism of inflammation sensitive drug delivery system.

2. Results and discussion

In order to implement inflammation responsive gatekeeping concept, we initially needed to develop some facile strategy to produce concentrated solution of water dispersed, biocompatible, and ultrasmall thiol stabilized quantum dots to cap drug loaded 3 nm wide pores of MSNs. Ultrasmall and high quality nanoparticles are conventionally synthesized in high boiling organic solvents. In the course of synthesis, nanoparticles are usually stabilized by hydrophobic ligands; and as a result, as-synthesized uniform nanoparticles can only

be dispersed in organic solvents. Water instability is highly inappropriate feature for biomedical applications, therefore laborious and intricate ligand exchange approaches are subsequently adopted to render them water soluble. Rather than using two phase synthesis, we have developed a rapid and facile water based synthetic strategy to produce ultrasmall ZnS quantum dots. 3-mercaptopropionic acid (MPA) is utilized as a stabilizer in the reaction medium to passivate aggregation prone ZnS QDs. Moreover, presences of free COOH groups provide conjugation sites for blocking the drug loaded amine functionalized MSNs. The resulting MPA stabilized ZnS QDs were evaluated using X-ray diffraction (XRD), Transmission Electron microscopy (TEM), Infra-red (IR) and X-ray photoelectron spectroscopy (XPS). TEM micrograph demonstrates a stable hydrosol of ZnS QDs, mostly spherical and highly monodispersed nanoparticles with a diameter of 3-4 nm can be seen; otherwise at room temperature and in water based synthesis large or agglomerates of small ZnS NPs are produced. The high-resolution TEM micrograph (Figure 4a) showed crystalline nature of the product with clear lattice fringes, similarly selected area electron diffraction (SAED) patterns also confirmed the crystallinity of ZnS QDs (Inset of Figure 4a). XPS analysis indicated the composition and purity of as-synthesized product; results substantiated the presence of Zn and S with atomic ratio of almost 1:1 (Figure S1).We also used powder XRD to probe the crystal structure, observed pattern suggested zinc blende structure with broad peaks to imply the generation of ultrasmall nanoparticles (Figure 1a). Surface functionalization was validated by zeta potential measurements, highly negative surface charge (-12 mV) of ZnS is observed, as displayed in Table S1. Optical properties of ZnS QDs were examined using UV-Vis and PL techniques. A prominent peak centered at 300 nm was noticed in UV−Vis spectrum (Figure 1b). Figure 1c illustrates the PL spectra of ZnS QDs scanned at room temperature; it displays a distinct peak at 425 nm when the sample is excited at a wavelength of 350 nm. Digital photograph of a thiol stabilized ZnS QDs suspension synthesized at room temperature showed highly transparent water stable product. Subsequently, the effect of different bio-relevant oxidants on the stability of ZnS QDs was assessed. Concentration of H_2O_2 was progressively increased from 1 to 50 mM, but the solution of ZnS QDs remained stable in such a strong oxidant environment, as shown in cuvettes 2 and 3 in Figure 1d. Surprisingly, addition of Fe^{2+}, the most plentiful transition-metal in the body, readily destabilized ZnS QDs at quite lower H_2O_2 concentrations due to the generation of highly reactive hydroxyl radicles (•OH). Mechanistically, thiol groups which stabilized ZnS nanolids are instantly oxidized by •OH and as a result aggregated product was appeared in cuvette 4. IR spectrum authenticated the MPA conjugation onto ZnS QDs; an intense and strong peak placed at 1710 cm^{-1} can be attributed to the C=O stretching mode of carboxylate groups, however the absence of typical free thiol peak at ~2490 cm^{-1} suggested the chemisorption of MPA onto the surface of ZnS QDs via Zn-thiol bond (Figure 2c).

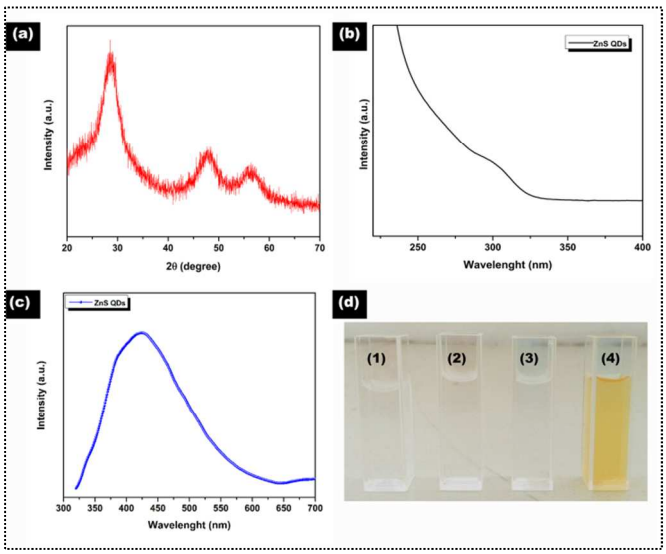

Figure 1. (a) High-angle XRD patterns of ZnS QDs. (b) Absorbance spectrum of mercaptopropanoic acid stabilized ZnS QDs. (c) Photoluminescent spectrum of ZnS QDs when excitation wavelength was 350 nm. (d) Digital photographs to demonstrate the quality of stabilized ZnS QDs and their interaction with different biorelevant oxidants, (1) ZnS-MPA QDs, (2) ZnS-MPA QDs+5 mM H_2O_2, (3) ZnS-MPA QDs+50 mM H_2O_2 (4) ZnS-MPA QDs+2 mM H_2O_2+Fe^{2+}

Meanwhile, porous nanocarrier was prepared using already established synthetic route. To enhance the grafting of amine (NH_2) moiety, both co-condensation and post grafting approaches were used. Empty channels of amine functionalized mesoporous silica nanoparticles (denoted as MSNs-NH_2) were filled with rhodamine 6G dye and anticancer drug camptothecin (CPT) as model cargo molecules to perform proof–of-concept studies. The loading amount of both guest were calculated, using UV/Vis spectroscopy. Finally, thiol-stabilized ZnS QDs were utilized as nanolids to prevent the premature release of loaded cargoes. Carbodiimide chemistry ensured the capping of drug loaded MSNs-NH_2 with carboxylate terminated ZnS QDs. Various analytical and spectroscopic techniques were then used to validate the gatekeeping phenomenon. Appearance of typical MCM-41-like peaks in low-angle XRD revealed a highly ordered hexagonal structure of MSNs-NH_2. Upon drug loading and pore capping, the intensity of peaks was markedly reduced, which was ascribed to the pore-filling and pore capping and thus decreased the scattering contrast between the pores and the framework of MSNs (Figure 2a). The nitrogen adsorption/desorption isotherms of MSNs formulations (MSN-NH_2, ZnS@Rhd@MSNs) were presented in Figure 2b. All isotherms were found to be type IV, which obviously indicated the presence of mesopores. The pore size distributions curves of MSN-NH_2 displayed a narrow pore size distribution centered at around of 3.2 nm (inset of Figure 2b), calculated using the BJH computation procedure. Expectedly, loading of cargo molecules led to reduction in surface area and pore volume from 887 m^2/g to 610m^2/g and 0.92 to 0. 59 cc/g respectively. That reduction suggested the placement of drug molecules within the pores of the MSNs rather than physically bound on the surface of MSNs. More significant reduction in surface area and pore

volume was noticed upon capping the drug loaded MSNs with ZnS QDs, the surface area and pore volume were dropped down to 20 and 0.12cc/g respectively.

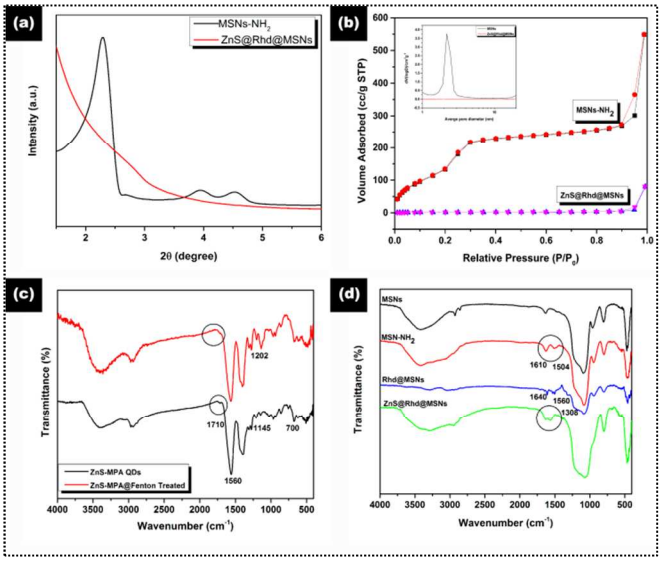

Figure 2. (a) Low-angle X-ray diffraction (XRD) patterns of MSN-NH_2.and ZnS@Rhd@MSNs. (b) Nitrogen adsorption–desorption isotherms and pore size distribution of MSN-NH_2 and ZnS@Rhd@MSNs. (c) FTIR spectra of mercaptopropanoic acid stabilized ZnS QDs and Fenton treated ZnS QDs. (d) FTIR spectra of MSNs, MSNs-NH_2, Rhd@MSNs and ZnS@Rhd@MSNs.

Moreover, IR spectra shed some light on the composition and surface modifications of synthesized nanoparticles; Figure 2c, d presents IR spectra of MSNs, MSNs-NH_2, Rhd@MSNs, ZnS@Rhd@MSNs, ZnS–MPA QDs and after Fenton treatment. Absorption bands found in MSN-NH_2 at 1610 and 1504 cm^{-1} were assigned to N–H bending (primary amines only), whereas no such bands were noticed in unfunctionalized MSNs. In, ZnS@Rhd@MSN sample, the vibrational band at ~960 cm^{-1} was associated with silanol groups (Si–OH) whereas ZnS QDs associated carboxylate peaks 1560 cm^{-1} (Stretching of OCO of MPA) validated the anchoring of ZnS QDs on MSNs surface, as can be seen in Figure 2d. Following hydroxyl radical exposure, typical mercapto bands (700 and 1145 cm^{-1}) were shifted to 1202 cm^{-1}, demonstrating the oxidation of SH to SO3H group through Fenton reaction. Moreover, in addition to thiol oxidation there is also another possibility that ZnS QDs could be etched /dissolved following the interaction with highly reactive •OH.

The morphologies of ordered MSN-NH_2 were visualized by SEM micrographs; Figure.3a indicates spherically shaped, uniform, smooth surfaced nanoparticles with a diameter of 100 nm. On the contrary, the surface of ZnS capped MSNs became rough after ZnS conjugation, which verified a successful anchorage of ultrasmall ZnS QDs onto the outlets of MSNs (Figure.3b). The resulting nanoparticles were subsequently exposed to 20mM H_2O_2 solution, but no apparent change in the morphology of ZnS@CPT@MSNs was observed , however, upon treating the drug loaded and ZnS capped MSNs with •OH, some additional nanostructures were observed in SEM images, as can be seen in Figure 3d. Emergence of extra structures can most probably be the aggregated ZnS QDs which are generated due to the oxidation of thiol groups. SEM associated Energy-dispersive X-ray (EDX) results (Figure S2) also ratified the existence of elemental Zn and S in MSNs with the atomic ratio of Zn:S equaling to 1.7:1 that was close to the stoichiometry of bulk ZnS. Furthermore, the signals of Si and O were assigned to porous silica which acted as a nanocarrier.

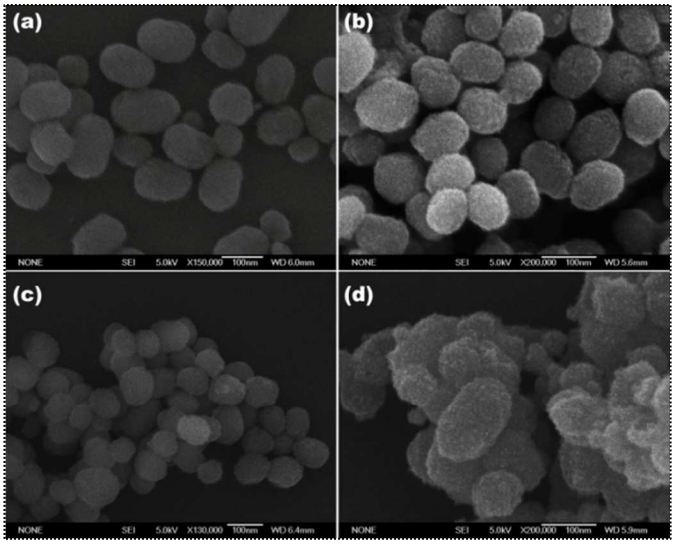

Figure 3. (a) SEM micrograph of MSNs-NH_2. (b) ZnS QDs capped MSNs. (c) Image is acquired after treatment of ZnS@Rhd@MSNs with 50 mM H_2O_2. (d) ZnS capped MSNs sample after 1 mM H_2O_2 in the presence of Fe^{2+}

TEM analysis was performed to further probe the nature of rough surfaced MSNs and generation of extra aggregated product; Figure 4b displays representative (TEM) image of monodispersed and uniform MSN-NH_2 nanoparticles with an average diameter of 100 nm. Nanoparticles possessed 2D hexagonal ordered array of mesopores which can be clearly seen at high resolution, moreover, the exterior surface of nanoparticles was found smooth without any contrast. When ZnS@CPT@MSNs sample was inspected, the surface of MSNs was significantly covered with ultrasmall dots, and hexagonal channels which were clearly visible in as synthesized MSNs sample, became invisible after ZnS QDs capping (Figure 4c). Substantial coverage of drug loaded nanocarriers suggested a successful and efficient capping of CPT@MSNs by ZnS QDs. TEM was also proved helpful in demonstrating the hydroxyl mediated uncapping of MSNs. Capped sample (ZnS@CPT@MSNs) was subjected to various concentrations of hydrogen peroxide solutions to oxidize thiol moieties. Exposure of as high as 20 mM H_2O_2 solution failed to separate ZnS from the surface of MSNs surface. But, biorelavent concentrations of H_2O_2 (250 µM) in the presence of free iron (Fe^{2+}) ensured the removal of ZnS QDs due to generation of highly reactive •OH. Unstabilized ZnS QDs were found in a crosslinked fashion presumably due to the establishment of disulfide bonds between quantum dots after thiol group oxidation, as can be seen in Figure 4e. With amplification of hydroxyl radicles, complete removal of ZnS QDs was observed

from the surface of MSNs (Figure 4f), thus opening the drug loaded nanochannels to release the cargo in a controlled fashion. Moreover, in case of high concentration of •OH, no extra or aggregated ZnS QDs were detected in TEM images, suggesting the complete dissolution of ZnS QDs.

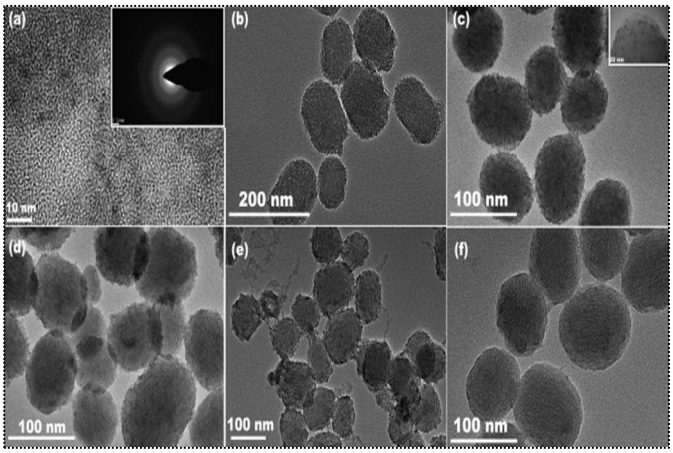

Figure 4. (a) HR-TEM image of mercaptopropanoic acid stabilized ZnS QDs, inset: Selected area electron diffraction (SAED) patterns of ZnS QDs. (b) TEM image of MSNs-NH_2. (c) ZnS capped MSNs nanocomposite. (d) TEM obtained after treating ZnS@MSNs with 20 mM H_2O_2. (e) ZnS capped MSNs sample after 250 µM H_2O_2 in the presence of Fe^{2+}. (f) ZnS capped MSNs sample after 2 mM H_2O_2 in the presence of Fe^{2+}

XPS is an effective analytical tool to determine the surface chemical composition and oxidation state of a sample, XPS survey spectrum (Figure 5a) indicated the presence of Zn, S, Si, O, and C peaks in ZnS@MSNs sample, which validated the conjugation of ZnS with silica matrix. The zinc peaks at Zn 2p 1/2 (1045 eV) and Zn 2p 1/3 (~1020 eV) showed the divalent oxidation state of zinc in ZnS QDs Figure 5b, whereas asymmetric peak at 163.3 eV can be ascribed to sulphide group (Figure 5c).As mentioned above, besides thiol oxidation there is a high possibility of dissolution or etching of ultrasmall ZnS QDs due to highly reactive nature of hydroxyl radicals. In order to probe ZnS QDs conjugation and dissolution phenomenon, we performed inductively coupled plasma mass spectrometry (ICP-MS) to detect the concentration of released Zn^{2+} ions following the treatment with different oxidants. Initially, a known amount of ZnS@MSNs sample was dissolved in nitric acid to determine the total extent of conjugated ZnS QDs. Capped sample was later exposed to different concentrations of H2O2 and hydroxyl radicals. The ICP results showed a significant etching/dissolution phenomnon when ZnS QDs interacted with •OH. The released amount of Zn^{2+} was found dependent on the concentration of •OH. With the amplification of hydroxyl radicles, a corresponding increase in the concentration of Zn^{2+} was noticed (Figure5d). Five millimolar H_2O_2 in the presence of Fe^{2+} was found enough to etch almost 70% ZnS QDs. On the other hand, very high concentrations of just H2O2 (without Fe^{2+}) are required to dissolve ZnS QDs. For instance, only 30% Zn^{2+} was released when ZnS@MSNs sample was exposed to 50mM H_2O_2.

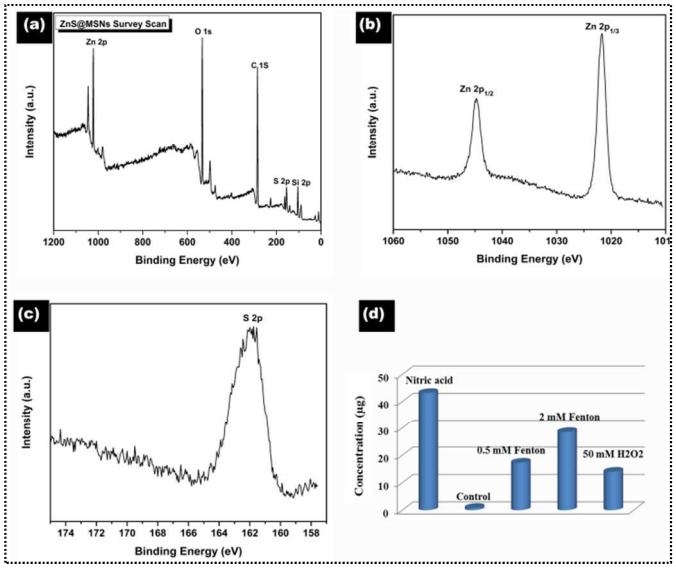

Figure 5. (a) XPS survey spectrum of ZnS@MSNs (b) spectrum of Zn 2p which validates the presence of elemental zinc in MSNs composite. (c) Spectrum of S 2p (d) inductively coupled plasma (ICP) analysis after exposing ZnS@MSNs sample to nitric acid and different concentration of vitamin H_2O_2 in the absence and presence of Fe^{2+}.

Camptothecin (CPT) is a well-known anticancer drug but with a very poor water solubility. On research front, it exhibited excellent in vitro efficacy, yet in vivo studies failed to produce encouraging results because of its hydrophobic nature. Use of nanocarriers to deliver water insoluble drugs is nowadays an extensively pursued that is why we also opted to load CPT in porous structure of MSNs and transport in a smart and controlled fashion. In order to evaluate the hydroxyl mediated controlled release of CPT; in vitro drug release experiments were carried. A specified amount of ZnS@CPT@MSNs was first dispersed in PBS then release kinetics was monitored over 3 days under various oxidant conditions. A slight amount of drug was detected in buffer solution (Without any trigger) that indirectly indicated a successful capping of CPT loaded nanopores of MSNs. Influence of ferrous salt (Fe^{2+}) on the drug release kinetics was also investigated. A known amount of Fe^{2+} was introduced into release medium, but the Figure 6a indicates that the addition of Fe^{2+} fails to cause any influence on the release rate. Sample was later exposed to higher concentrations of H_2O_2, but release amount remained almost unchanged, suggesting the stability of thiol group against H_2O_2. As high as 20 mM H_2O_2 failed to oxidize a significant amount of thiol groups. In contrast, the presence of both Fe^{2+} and H_2O_2 caused a positive impact on release rate, as can be seen in Figure 6a. The underlying reason behind such reactivity stemmed from the generation of more reactive •OH that readily oxidize thiol groups. Since in this study ZnS nanocaps were stabilized by thiol groups, therefore in-situ generated •OH readily oxidized thiol groups to open loaded nanochannels of MSNs to sustainably release CPT molecules. One millimolar H_2O_2 in the presence of iron was found sufficient to oxidize thiol groups

and thus allow the release of loaded CPT molecules. With increasing •OH, the amount of released CPT is correspondingly increased, as shown in Figure 6a.

Besides anticancer drug, release of rhodamin 6G dye from ZnS capped MSNs was also monitored in the presence of different reactive oxygen species. Figure 6b displays the release profile of rhodamin 6G dye from ZnS@Rhd@MSNs sample under the similar conditions which were applied to CPT System. Release profile of rhodamin 6G toes almost a similar pattern as was observed in case of CPT.

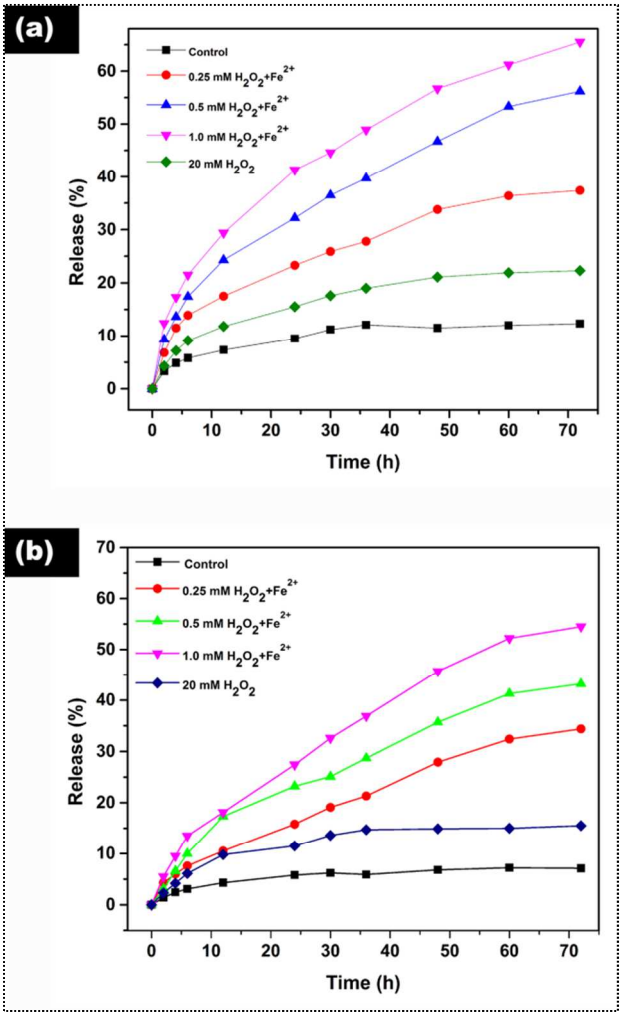

Figure 6. (a) Release profile of camptothecin from ZnS@CPT@MSNs sample in the absence and presence of different concentrations of H_2O_2 (0.25, 0.5, 1.0 and 20.0 mM) with and without Fe^{2+}. (b) Release profile of rhodamin 6G from ZnS@Rhd@MSNs formulation after exposing to different concentrations of H_2O_2 (0.25, 0.5, 1.0 and 20.0mM) in the presence and absence of Fe^{2+}.

To estimate the therapeutic effectiveness of CPT loaded nanoformulation, in vitro cell viability of model pancreatic cancer cells (BxPC-3) was assessed using various concentrations of MSNs nanoformulations (0–100 µg/mL of MSN) through MTT [3-(4,5-dimethylthiazol-2-yl)-2,5-diphenyltetrazolium bromide viability assay. The assay uses the activity of mitochondrial dehydrogenase enzyme, which in living cells breaks the yellow MTT salt into purple colored formazan product, to calorimetrically monitor the number of viable cells. No significant reduction in cell viability was observed following 48 h incubation of MSN-NH_2 and ZnS-MSN, demonstrating the biocompatible nature of nanocarrier and nanocomposite (Figure 7).

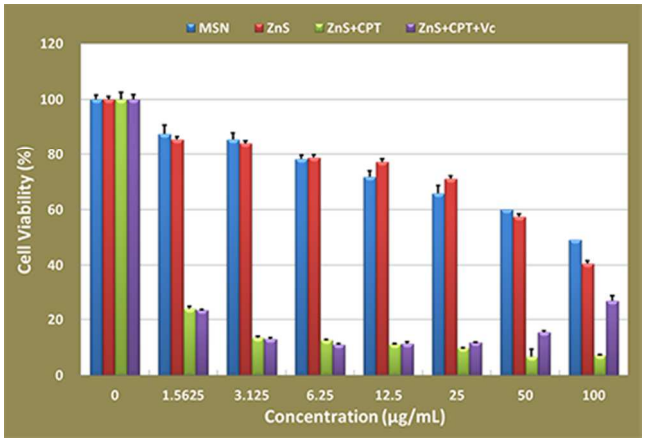

Figure 7. (a)In vitro viability of BxPC-3 cells in the presence of different concentrations of MSNs-NH_2, ZnS@MSNs, ZnS@CPT@MSNs and ZnS@CPT@MSNs nanoformulations with vitamin C, the incubation time was 48 h.

When ZnS capped and CPT loaded nanoformulation (ZnS@CPT@MSNs) was added into cell culture for 48 h, the cell viability count was significantly decreased and almost 80% cells were found dead at as low as 1.56 µg/mL. It should be kept in mind that 1.56 µg/mL is the weight of drug loaded nanocomposite not just drug molecules. Such an impressive chemotoxicity can be attributed to the controlled release of loaded CPT molecules, which is only possible if ZnS nanocaps are detached from the surface of pores. Abovementioned characterization techniques have already excluded the involvement of just H_2O_2 in the oxidation of ZnS QDs stabilizing thiol groups; however intracellularly produced hydroxyl radicles possibly oxidizes the thiol groups which in turn opens the nanopores due to detachment of ZnS nanocaps. As far as hydroxyl production in cancer cells goes, it is well recognized that cancer cells produce inordinate ROS level due to increased metabolic needs and mitochondrial dysfunction. Analogously, inflammation, which is a critical component of tumor progression, also induces oxidative stress in cancer microenvironment. Likewise, there is mounting evidence which indicates a significantly high iron demand of malignant cells to meet their rapid cell division.[54-57] Taken together, anomalous surge in ROS and iron levels probably results in the generation of excessive amount of hydroxyl radicles. In order to further confirm the role of ROS mediated drug release, BxPC-3 cells were also treated with 20 µg/mL vitamin C, serves as antioxidant to detoxify intracellular ROS. It was observed that incubation of vitamin C had a negative impact on the effectiveness of cytotoxic drug. Cell growth inhibitory effect was relatively reduced in the presence of ROS scavenger, as

can be seen in Figure 7 which shows a higher cell counts than without vitamin C group. Hence, we can safely maintain that intracellular ROS most likely oxidize thiol group of ZnS nanocaps and resulting destabilization of ZnS QDs unlock o CPT loaded nanochannels of MSNs for controlled release.

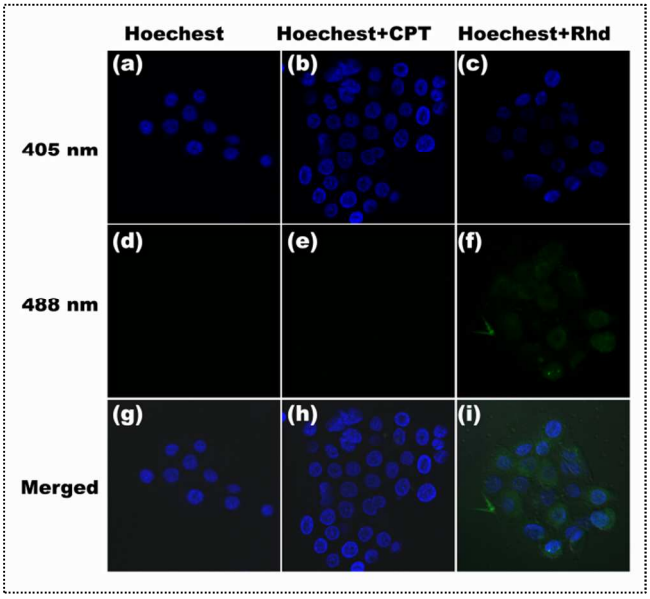

Figure 8. CLSM micrographs of BxPC-3 cells after 5 h incubation with ZnS@CPT@MSNs and ZnS@Rhd @MSNs (50 µg/mL). Cells nucleus are stained with Hoechest dye (a,d,g). While, b,e,h images shows cells which are incubated with Hoechest dye and ZnS@CPT@MSNs nanoformulation. Micrographs c,f,i displays cells treated with Hoechest dye and ZnS@Rhd@MSNs nanoformulation.

Confocal microscopy was used to determine the intracellular uptake and responsive drug release by incubating the BxPc-3 cells with definite amount of ZnS@CPT@MSNs and ZnS@Rhd@MSN. Nucleus of cells were first stained with Hoechst dye; blue color was clearly visible in the nuclear area of stained cells. Following 5 h incubation of CPT loaded sample (50 µg /ml), more intense blue dotted luminescence was observed in the cytoplasmic regions because of blue-colored fluorescent CPT, indicating the cellular uptake of drug loaded nanoparticles (Figure 8). Dye loaded samples can provide a better contrast, therefore, rhodamin 6G loaded sample (ZnS@Rhd@MSNs) was also tried to proof responsive and controlled drug release system. In this scenario, in addition to blue-stained nucleus, Figure8 shows greenish fluorescence in the cytoplasmic regions, indicating the responsive release of dye molecules.

3. Conclusions

In summary, we presented a hydroxyl radical mediated drug delivery system for transporting anticancer drugs specifically to oxidative stressed microenvironment. Ultrasmall thiol passivated ZnS NPs were used to clog the drug loaded nanochannels of porous silica. Exposure of hydroxyl radicals resulted in the oxidation of thiol group, thus destabilizing the ZnS nanolids to open the drug encompassing pores. Cell viability study exhibited an excellent anticancer activity, whereas confocal imaging verified cellular uptake and responsive release behavior of resulting nanoformulation. Moreover, unique porous structure of MSNs enabled us to use this platform to load dyes, which could be served as sensor to detect ROS. The development of nanocarrier that responds to oxidative environments, found in cancer or inflammatory sites, to release therapeutic entities in a controlled fashion holds a great potential for treating various oxidative stress related pathological conditions.

Acknowledgements

We are grateful to the financial support from National Basic Research Program of China (973 Program, grant nos.2012CB821700), Major International (Regional) Joint Research Project of NSFC (grant nos. 21120102034) NSFC (grant nos.20831002) and Australian Research Council Future Fellowship (FT100101059).

Notes and references

[a] State Key Laboratory of Inorganic Synthesis and Preparative Chemistry, College of Chemistry, Jilin University, Changchun, 130012, China.
[b] College of Life Science, Jilin University, Changchun, 130012, China
[c] China Japan Union Hospital, Jilin University, Changchun, 130031, China.
Corresponding author: zhugs@jlu.edu.cn, djs3043@126.com.

Electronic Supplementary Information (ESI) available: [experimental methods, materials, characterization, Figure (S1 &S2) and Table S1] See DOI: 10.1039/b000000x/

1. H. J. Forman and M. Torres, *Am. J. Respir. Crit. Care Med.* 2002, **166**, S4-S8.
2. R. Kohen and A. Nyska, *Toxicol Pathol.* 2002, **30**, 620-650.
3. Y. Yang, A. V. Bazhin, J. Werner and S. Karakhanova, *Int. Rev. Immunol.* 2013, **32**, 249-270.
4. G. M. Rosen, S. Pou, C. L. Ramos, M. S. Cohen and B. E. Britigan, *The FASEB J.* 1995, **9**, 200-209.
5. P. S. Hole, R. L. Darley and A. Tonks, *Blood*, 2011, **117**, 5816-5826.
6. M. Valko, C. J. Rhodes, J. Moncol, M. Izakovic and M. Mazur, *Chem. Biol. Interact.* 2006, **160**, 1-40.
7. C. Gorrini, I. S. Harris and T. W. Mak, *Nat. Rev. Drug. Discov.* 2013, **12**, 931-947.
8. R. M. Touyz, *Hypertension*, 2004, **44**, 248-252.
9. S. J. Nicholls and S. L. Hazen, *Arterioscler. Thromb. Vasc. Biol.* 2005, **25**, 1102-1111.
10. D. Roos and C. C. Winterbourn, *Science*, 2002, **296**, 669-671.
11. C. Vives-Bauza, R. Gonzalo, G. Manfredi, E. Garcia-Arumi and A. L. Andreu, *Neurosci. Lett.* 2006, **391**, 136-141.
12. H. Sies, *Exp. Physiol.* 1997, **82**, 291-295.
13. T. Finkel and N. J. Holbrook, *Nature*, 2000, **408**, 239-247.
14. R. A. Floyd, *Exp. Biol. Med.* 1999, **222**, 236-245.
15. T. Ozben, *J. Pharm. Sci.* 2007, **96**, 2181-2196.
16. A. T. Y. Lau, Y. Wang and J.-F. Chiu, *J. Cell. Biochem.* 2008, **104**, 657-667.
17. H. M. Hassan and I. Fridovich, *Arch. Biochem. Biophys.* 1979, **196**, 385-395.
18. A. Boveris, N. Oshino and B. Chance, *Biochem. J.* 1972, **128**, 617-630.
19. S. G. Rhee, T.-S. Chang, Y. S. Bae, S.-R. Lee and S. W. Kang, *J. Am. Soc. Nephrol*. 2003, **14**, S211-S215.

20. S. G. Rhee, Y. S. Bae, S.-R. Lee and J. Kwon, *Sci. STKE*, 2000, **2000**, pe1-.
21. R. H. Burdon, *Free Radic. Biol. Med.* 1995, **18**, 775-794.
22. L. P. Candeias, K. B. Patel, M. R. L. Stratford and P. Wardman, *FEBS Lett.* 1993, **333**, 151-153.
23. S. J. Weiss, G. W. King and A. F. LoBuglio, *J. Clin. Invest.* 1977, **60**, 370-373.
24. B. Halliwell and J. M. C. Gutteridge, in *Meth. Enzymol*. ed. A. N. G. Lester Packer, Academic Press1990, vol. Volume 186, pp. 1-85.
25. B. Lipinski, *Oxid. Med. Cell. Longev*. 2011, **2011**.
26. J. M. C. Gutteridge, *Ann. N. Y. Acad. Sci.*1994, **738**, 201-213.
27. S. Puntarulo, *Mol. Aspects. Med.* 2005, **26**, 299-312.
28. *Nutr. Rev.* 2004, **62**, 120-124.
29. J. M. McCord, *Science*, 1974, **185**, 529-531.
30. S. J. Weiss, P. K. Rustagi and A. F. LoBuglio, *J. Exp. Med.* 1978, **147**, 316-323.
31. D. C. Malins, S. J. Gunselman, E. H. Holmes and N. L. Polissar, *Cancer*, 1993, **71**, 3036-3043.
32. S. V. Torti and F. M. Torti, *Nat. Rev. Cancer*, 2013, **13**, 342-355.
33. L. M. Coussens and Z. Werb, *Nature*, 2002, **420**, 860-867.
34. G. Waris and H. Ahsan, *J. Carcinog.* 2006, *5*, 14
35. B. N. Ames, M. K. Shigenaga and T. M. Hagen, *Proc. Natl. Acad. Sci.* 1993, **90**, 7915-7922.
36. K. B. Beckman and B. N. Ames, *J. Biol. Chem.* 1997, **272**, 19633-19636.
37. K. K. Jain, *Nanomedicine (Lond)*, 2009, **4**, 249-252.
38. M. E. Davis, Z. Chen and D. M. Shin, *Nat. Rev. Drug. Discov*. 2008, **7**, 771-782.
39. S. Mura, J. Nicolas and P. Couvreur, *Nat. Mater*. 2013, **12**, 991-1003.
40. S.-M. Lee and S. T. Nguyen, *Macromolecules*, 2013, **46**, 9169-9180.
41. M. Vallet-Regí, F. Balas and D. Arcos, *Angew. Chem. Int. Ed.* 2007, **46**, 7548-7558.
42. J. L. Vivero-Escoto, I. I. Slowing, B. G. Trewyn and V. S. Y. Lin, *Small*, 2010, **6**, 1952-1967.
43. F. Muhammad, M. Guo, W. Qi, F. Sun, A. Wang, Y. Guo and G. Zhu, *J. Am. Chem. Soc.*, 2011, **133**, 8778-8781.
44. Z. Luo, K. Cai, Y. Hu, L. Zhao, P. Liu, L. Duan and W. Yang, *Angew. Chem. Int. Ed.* 2011, **50**, 640-643.
45. Y. Zhu, H. Liu, F. Li, Q. Ruan, H. Wang, M. Fujiwara, L. Wang and G. Q. Lu, *J. Am. Chem. Soc.*, 2010, **132**, 1450-1451.
46. N. K. Mal, M. Fujiwara and Y. Tanaka, *Nature*, 2003, **421**, 350-353.
47. C. R. Thomas, D. P. Ferris, J.-H. Lee, E. Choi, M. H. Cho, E. S. Kim, J. F. Stoddart, J.-S. Shin, J. Cheon and J. I. Zink, *J. Am. Chem. Soc.*, 2010, **132**, 10623-10625.
48. K. E. Broaders, S. Grandhe and J. M. J. Fréchet, *J. Am. Chem. Soc.*, 2010, **133**, 756-758.
49. A. Napoli, M. Valentini, N. Tirelli, M. Muller and J. A. Hubbell, *Nat. Mater*. 2004, **3**, 183-189.
50. E. A. Mahmoud, J. Sankaranarayanan, J. M. Morachis, G. Kim and A. Almutairi, *Bioconjug. Chem.* 2011, **22**, 1416-1421.
51. P. Han, N. Ma, H. Ren, H. Xu, Z. Li, Z. Wang and X. Zhang, *Langmuir*, 2010, **26**, 14414-14418.
52. D. Trachootham, J. Alexandre and P. Huang, *Nat. Rev. Drug. Discov*. 2009, **8**, 579-591.
53. H. Pelicano, D. Carney and P. Huang, *Drug Resist. Update.* 2004, **7**, 97-110.
54. G. Nie, G. Chen, A. D. Sheftel, K. Pantopoulos and P. Ponka, *Blood*, 2006, **108**, 2428-2434.
55. D. R. Richardson, *Critical Reviews in Oncology/Hematology*, 2002, **42**, 267-281.
56. D. R. Richardson, D. S. Kalinowski, S. Lau, P. J. Jansson and D. B. Lovejoy, *Biochim. Biophys. Acta,* 2009, **1790**, 702-717.
57. D. S. Kalinowski and D. R. Richardson, *Pharmacol. Rev.* 2005, **57**, 547-583.

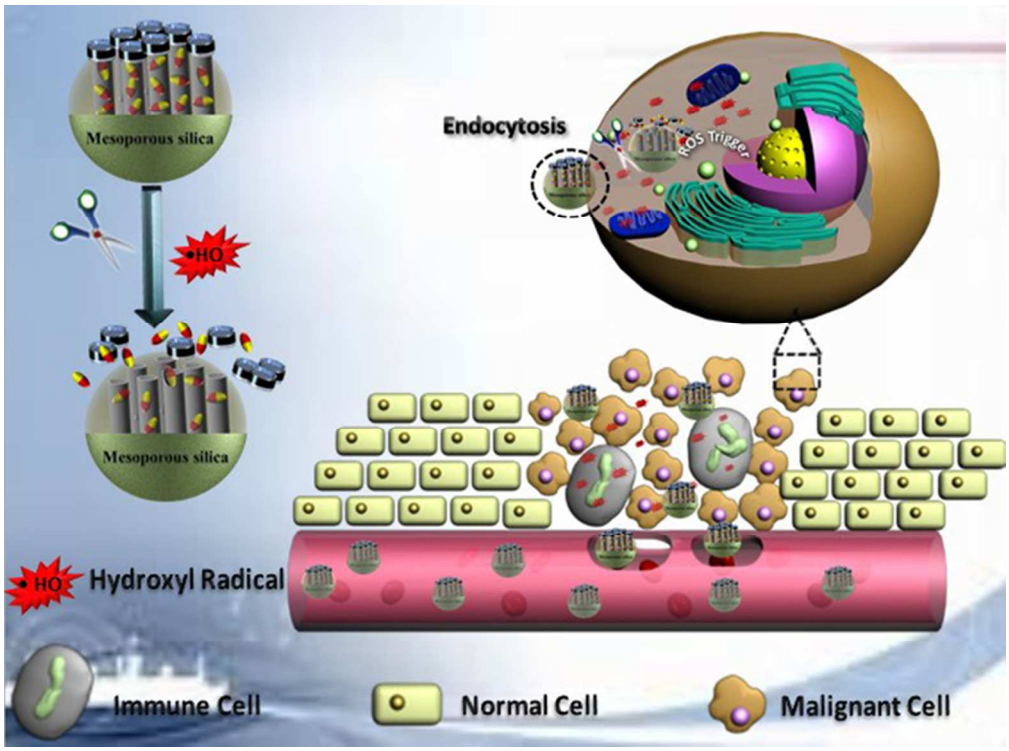

75x55mm (300 x 300 DPI)